Article

Stiffening of Red Blood Cells Induced by Cytoskeleton Disorders: A Joint Theory-Experiment Study

Lipeng Lai,[1,2] Xiaofeng Xu,[1,3] Chwee Teck Lim,[1,3,4,5] and Jianshu Cao[1,2,*]

[1]Singapore-Massachusetts Institute of Technology Alliance for Research and Technology Centre, Singapore; [2]Department of Chemistry, Massachusetts Institute of Technology, Cambridge, Massachusetts; [3]National University of Singapore Graduate School for Integrative Sciences and Engineering, [4]Nano Biomechanics Laboratory, Department of Biomedical Engineering and Department of Mechanical Engineering, and [5]Mechanobiology Institute, National University of Singapore, Singapore

ABSTRACT The functions and elasticities of the cell are largely related to the structures of the cytoskeletons underlying the lipid bilayer. Among various cell types, the red blood cell (RBC) possesses a relatively simple cytoskeletal structure. Underneath the membrane, the RBC cytoskeleton takes the form of a two-dimensional triangular network, consisting of nodes of actins (and other proteins) and edges of spectrins. Recent experiments focusing on the malaria-infected RBCs (iRBCs) show that there is a correlation between the elongation of spectrins in the cytoskeletal network and the stiffening of the iRBCs. Here we rationalize the correlation between these two observations by combining the wormlike chain model for single spectrins and the effective medium theory for the network elasticity. We specifically focus on how the disorders in the cytoskeletal network affect its macroscopic elasticity. Analytical and numerical solutions from our model reveal that the stiffness of the membrane increases with increasing end-to-end distances of spectrins, but has a nonmonotonic dependence on the variance of the end-to-end distance distributions. These predictions are verified quantitatively by our atomic force microscopy and micropipette aspiration measurements of iRBCs. The model may, from a molecular level, provide guidelines for future identification of new treatment methods for RBC-related diseases, such as malaria infection.

INTRODUCTION

The mechanical properties of a system are largely dictated by its structure. The property-structure relationship has been studied extensively in different fields in physics and engineering (e.g., Discher et al. (1), Suresh (2), and Broedersz and MacKintosh (3), etc.). In recent years, networks in biological systems have drawn much attention due to their close relationships to the functions of organisms. Example systems of biopolymer networks are cytoskeletons in various cells, which can be quasi-one-dimensional (e.g., axons of neuron cells (4,5)), two-dimensional (e.g., red blood cells (RBCs)), or three-dimensional. A biopolymer network can behave very differently from a network made of synthesized polymers. Firstly, biopolymer networks can be active with the participation of ATPs (J. H. Kim and J. Cao, unpublished data). Secondly, the components of a biopolymer network usually follow the wormlike chain (WLC) behavior, whose elasticity has an entropic origin and thus a nonlinear dependence on the end-to-end distance of corresponding biofilaments.

On the cellular level, the biological functions and behaviors of cells are related to their mechanical properties (2,6). The mechanical properties of cytoskeletons and membranes have been studied intensively in different scenarios, via experiments (e.g., Discher et al. (1), Lenormand et al. (7), and Hale et al. (8)), simulations (e.g., Saxton (9), Boal (10), Hansen et al. (11), and Boey et al. (12)), and theoretical models (e.g., Broedersz and MacKintosh (3) and Gov (13)). In addition, the membrane of RBCs is also investigated carefully from both biological and physical perspectives, including the functions of transmembrane proteins, and the interactions between protein complexes and the spectrins in the cytoskeletal network (e.g., Gov (13) and Byers and Branton (14)), etc. As an example to illustrate the relationship between the mechanical properties of the membranes and the behavior of the cells, earlier studies showed that the adhesiveness, and hence the mobility of RBCs, is strongly affected by the stiffness of the membrane (including the lipid bilayer and the cytoskeleton) (15,16). Relating to this article, recent experiments reveal that the stiffening of RBC after being infected by malaria parasites (17-20) correlates with the structural transformation in the cytoskeleton of the infected RBCs (iRBCs) (21).

A similar correlation was also observed in iRBCs after chloroquine treatment. In both cases, it is found that, when RBCs were infected by malaria or iRBCs were treated with chloroquine, the shear modulus of the membrane increased with time. Meanwhile, the average length of the spectrins that formed the cytoskeletal network was increased. It is also noticed that the cytoskeleton mesh became more irregular with large holes that were absent in the cytoskeleton of normal RBCs, creating a broad

Submitted February 23, 2015, and accepted for publication October 20, 2015.

*Correspondence: jianshu@mit.edu

Editor: Simon Scheuring.

0006-3495/15/12/2287/8

http://dx.doi.org/10.1016/j.bpj.2015.10.036

distribution of hole sizes and spectrin lengths. It is known that the adhesiveness of iRBCs is one of the reasons that lead to the fatality of malaria infection (22). Because the stiffness of RBCs largely affects the adhesiveness of the cells, having a fundamental understanding of the relationship between the network structure and the macroscopic elastic properties will provide us with guidance in potentially discovering new drug targets or treatment methods.

In this study, we focus on rationalizing the correlation between the two experimental observations mentioned above and investigate how the structural changes at the molecular level affect the mechanical properties at the cellular level. We present both numerical solutions and analytical approximations based on a model combining the WLC description for single filaments and the effective medium theory (EMT). We use the cytoskeletal network of the RBC, approximated by a two-dimensional (2D) triangular network, to demonstrate any agreement between the model and the experiments. This study not only provides a further understanding of the relationship between structures and functions, but also provides a critical experimental test of the theoretical predictions. In addition, because our model is constructed with a general framework, it is expected that it can also be applied to other scenarios, such as three-dimensional networks of the cytoskeletons in other types of cells, designing of new biomaterials, etc.

MATERIALS AND METHODS

Experiments

Cell culture and enrichment

Common laboratory *Plasmodium falciparum* 3D7 parasites were used for the study. Parasite iRBCs were cultured in vitro following a conventional protocol (23). Culture stage synchrony was maintained using sorbitol treatment (24) and the early trophozoite stage iRBCs were used for the following experiments.

Atomic force microscopy experiment

Sample preparation. The atomic force microscopy (AFM) imaging samples were prepared following protocols similar to those used previously in Shi et al. (21). Briefly, synchronized and magnetic-activated cell sorting-enriched (24) early trophozoite stage malaria iRBCs after different hours of 1 μM chloroquine treatment (0, 4, 8, 16, and 24 h) were loaded on PHA-E-coated coverslips and then incubated for 4 h to allow sufficient contact time for iRBCs to adhere to the substrate and avoid whole cell detachment in the shear-wash step. Eighty milliliters of 5P8-10 buffer were used to shear-wash the iRBCs adhered to PHA-E-coated coverslips at an angle of ~20° by syringe, leaving only the tightly bounded membranes. The tight binding between membrane and substrate also maximally ensured the structure of the cytoskeleton remained in situ. The cytoplasmic-surface-exposed samples were checked under a phase-contrast microscope (model No. X71, Olympus, Melville, NY) and then vacuum-dried before imaging using AFM (see Fig. S1 in the Supporting Material).

AFM imaging. AFM imaging was carried on a Nanowizard atomic force microscope (JPK Instruments, Carpinteria, CA) with a tapping mode (air) using an SSS-NCHR AFM tip (NanoSensors, Santa Clara, CA) with a tip radius of 2 nm, and a Dimension FastScan atomic-force microscope (Bruker, Billerica, MA) with a Fast Scan AFM tip and a tip radius of 5 nm. Images were captured at the resolution of 512 × 512 pixels for 10 × 10 μm or 1 × 1 μm at a scan rate of 0.5–1 Hz depending on the scan scale and image quality. Approximately 10 iRBCs were scanned for each chloroquine treatment condition and a well-connected spectrin area was selected to represent the cell for data collection of spectrin lengths. A quantity of 10–30 spectrin lengths was collected from each cell and averaged to represent the spectrin length of that cell.

Measurement of the spectrin length. The spectrin length was measured as described previously in Shi et al. (21). As shown in Fig. S2, *a* and *b*, white lines that were traced along the spectrins between two junctions were measured as the spectrin lengths.

Micropipette experiment

Different durations of chloroquine-treated malaria iRBCs were prepared at a ratio of 1:2000 (cell pellet: 1% BSA (bovine serum albumin) solution in PBS (phosphate-buffered saline). A quantity of 400–600 μL of the diluted sample was pipetted into a home-made micropipette aspiration microscope cell holder that was mounted on the X71 microscope stage (Olympus) using masking tape. Borosilicate glass tubings (Sutter Instrument, Novato, CA) were pulled using a model No. 2000 micropipette puller (Sutter Instrument), then forged and cut into a micropipette tip with an inner diameter of 1–2 μm using a Microforge (Narashige, East Meadow, NY). A syringe pump was used to apply a negative suction pressure to aspirate the iRBC into the micropipette. A simple relationship between elongation of cell membrane aspirated into the micropipette and the applied negative pressure is given by (17)

$$\left(\Delta P \times D_p\right)/\mu = 2.45 \times \Delta L_p/D_p, \tag{1}$$

with $\Delta L_p/D_p > 1$, where ΔP is the applied negative pressure, D_p is the micropipette inner diameter, μ is the membrane shear elastic modulus, and ΔL_p is the aspirated length of the cell membrane into the micropipette. A number of image series were captured using a charge-coupled device camera every 1 s. By measuring the aspirated length and the applied negative pressure, the membrane shear modulus was obtained.

Irregular network of WLCs

Normal RBC possesses a triangular cytoskeletal network consisting of nodes of protein complexes and edges of spectrins. In our theoretical study of the RBC cytoskeleton, we regard the network formed by equilateral triangles as the regular network. We treat this regular network as our reference state and study how disorders added to the network affect its elasticity.

Recent experiments (21) find that in malaria-infected RBCs (iRBCs) or iRBCs after drug (chloroquine) treatment, two types of disorders are introduced to the RBC cytoskeletal network (Fig. 1). Firstly, the average end-to-end distance of the spectrins increases, which is directly measured in our experiment (Fig. 2 *b*). Secondly, the variance of the end-to-end distance distribution is also much larger than that in the regular triangular network (Fig. 2 *b* and Shi et al. (21)), probably due to the absence of some spectrin links after infection or drug-treatment. To perform a quantitative investigation of how these two changes affect the stiffness of the RBC network, we introduce the disorders in terms of a Gaussian distribution of the spectrins' end-to-end lengths z in the network, for which the probability density function can be written as

$$\widetilde{\mathcal{P}}(z) = \frac{C}{\sqrt{2\pi}\sigma} e^{-\frac{(z-z_0)^2}{2\sigma^2}} \; 0 < z < L. \tag{2}$$

Here, L is the natural length of the spectrins following the WLC description elaborated later, z_0 is the average end-to-end length of the spectrins, σ^2 is the variance of the end-to-end length distribution, and C is a normalization constant.

Each node in the network formed by protein complexes defines a point connecting the cytoskeleton and the membrane. In the regular network,

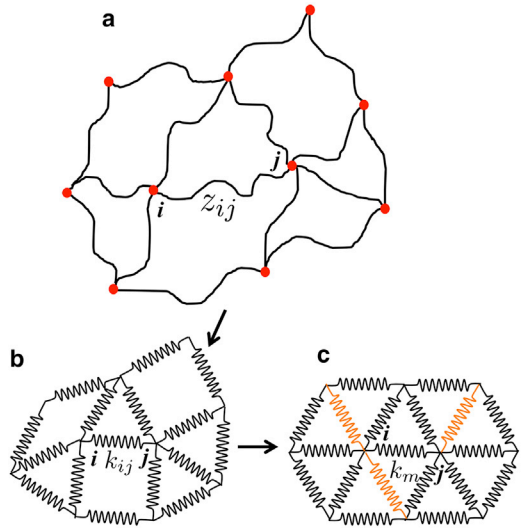

FIGURE 1 Sketches of the model. (*a*) A sketch of the 2D triangular network with disorders, resembling the cytoskeleton structure of the RBC (or iRBC). The lengths z_{ij} between two nodes are nonuniform and some connections are missing comparing to a regular network. (*b*) Based on the WLC model (Eqs. 3 and 4), the length variation in z_{ij} is mapped to the variation in the equivalent spring constant k_{ij} for small perturbations. (*c*) An EMT is applied to reduce the disordered network to a regular network with uniform spring constant k_m, from which the macroscopic in-plane shear modulus can be calculated. To see this figure in color, go online.

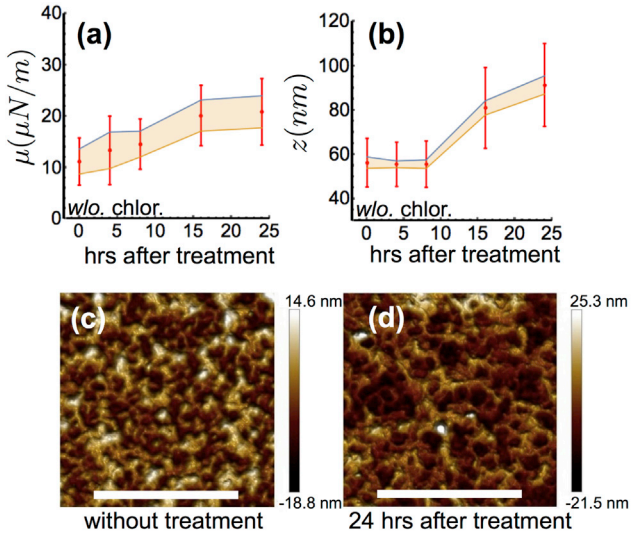

FIGURE 2 Experimental results. (*a*) Shear modulus μ as a function of the time after chloroquine treatment. (*b*) The end-to-end distance z as a function of the time after the treatment. In both (*a*) and (*b*), 0 h data correspond to cells without chloroquine treatment. (*Shaded areas* between the *blue* and *orange curves* in *a* and *b* indicate the 90% pointwise confidence band for the mean values, respectively.) (*c* and *d*) Typical images from AFM at different stages of the treatment (without chloroquine treatment for *c* and 24 h after the treatment for *d*). (*Color*) Relative height of the corresponding point. The scale bar in (*c*) and (*d*) is 1 μm. To see this figure in color, go online.

each node is linked by six spectrins, i.e., an out-degree of 6. But in reality, some spectrins may lose the connections with the nodes, which introduce a topological disorder to the network. Here we use a parameter p to represent the probability with which an edge of spectrin is present in the regular network (then $1-p$ represents the probability with which an edge of spectrin is missing from the regular network). For example, $p = 1$ corresponds to the complete network, and $p = 2/3$ corresponds to an average out-degree of 4. In our model, we generally treat p as an independent variable. But it is possible that p can be a function of stresses in the network as suggested by previous studies focusing on the binding/unbinding kinetics between ligands and receptors (e.g., Bell (25)). This case is further remarked in the Discussion section.

For individual spectrins, it is well known that the elasticity has an entropic origin. Here, we apply the WLC model that is used to study semiflexible polymers (e.g., Marko and Siggio (26), Yang et al. (27), and Xu et al. (28)) to single spectrins, which basically gives us a nonlinear force-extension curve (26). Comparing to the end-to-end distance of the spectrins in the network (~50 nm), the persistence length (l_p ~ 10 nm) of the spectrin is very short. Hence we need not consider the effect of the spectrins' bending rigidity on the network. For a brief review, in the WLC model, the persistence length l_p describes the length scale, below which the bending energy dominates the thermal excitations. From the WLC model, the single spectrin follows the force-extension relation as shown below (26),

$$\beta l_p f = \frac{z}{L} + \frac{1}{4(1-z/L)^2} - \frac{1}{4}, \tag{3}$$

where $\beta = 1/k_B T$ is the Boltzmann factor with k_B the Boltzmann constant and T is the temperature; z is the end-to-end distance of the spectrin; and L ~ 200 nm is the natural length of the spectrin that is treated as inextensible. With L ~ 200 nm and L_p ~ 10 nm, the root-mean-square end-to-end distance of a spectrin free of stress is ~60 nm, comparable to observed values. In general, the spectrins in the RBC cytoskeleton have an average end-to-end distance ranging ~50–100 nm. With small perturbations to the spectrin from its equilibrium position, we can expand the force-extension relation (Eq. 3) to first order and obtain an effective spring constant k for the spectrin, which is a function of the end-to-end distance z of the spectrin at equilibrium. Simply, this extension-related spring constant k is obtained by taking the derivative of the force with respect to the extension, which gives us

$$k(z) = \frac{\partial f}{\partial z} = \left(1 + \frac{1}{2}\left(1 - \frac{z}{L}\right)^{-3}\right) \Big/ \beta l_p L. \tag{4}$$

Importantly, we should note here that, even though the effective spring constant k depends on the end-to-end distance z nonlinearly, its effect in our model is simply to set up an initial equilibrium distribution of the spring constants across the entire network according to the distribution of the end-to-end distance of the spectrins. Under this assumption, we focus on the linear response of the disordered network (small perturbations), in which case each spectrin is treated as a Hookean spring with a distinct spring constant and then we apply an EMT to evaluate the elasticity of the disordered network.

Effective medium theory

To understand how the disorders in the RBC cytoskeleton affect its stiffness, we adopt an EMT approach here. In previous studies, EMT is used to understand the elastic properties of different types of disordered networks. Examples include but are not limited to central-force spring networks (29,30), 2D networks under tension (31-33), networks at large deformations (34), networks formed by filaments with finite bending rigidities (35,36), networks with nonlinear cross-linkers (37), etc. Basically, the EMT maps the disordered network to an equivalent regular network and extracts elastic constants from the regular network. To construct the

equivalent regular network, the springs in the network with distinct spring constants are replaced by springs with the same spring constant k_m self-consistently. The self-consistency requires that the average extra displacement δu caused by this replacement procedure must be 0 over the entire network ($\langle \delta u \rangle = 0$) (29). It leads to the following equation for the effective spring constant in the regular network (29),

$$\int \frac{\mathcal{P}(k)}{1-\alpha(1-k/k_m)}dk = 1, \quad (5)$$

where $\mathcal{P}(k)$ describes the distribution of the spring constants in the network. The value α is related to the topology of, and prestresses in, the network (31) and can be understood as follows: when two adjacent nodes in the regular network are displaced with respect to each other, the response of the network can be described by an effective spring constant $K' = k_m/\alpha$, where $0 < \alpha < 1$ takes into account the contribution of the whole network. Equation 5 can be solved analytically for specific probability density functions $\mathcal{P}(k)$ and numerically for other forms of $\mathcal{P}(k)$.

RESULTS

Experimental measurements

In the cytoskeleton of normal RBCs, the average end-to-end distance of the spectrins, i.e., the average distance between nodes, is ~50–60 nm. Here we summarize our experimental measurements using AFM and micropipette aspiration techniques. The measurements show correlation between the stiffening of the iRBC after chloroquine treatment as well as elongation of spectrins, which motivates our theoretical model.

The shear modulus of the iRBC is measured by micropipette aspiration (38,39). Fig. 2 *a* shows that the shear modulus of iRBC increases by an approximate factor of 2 after 24 h of chloroquine treatment. The cytoskeleton structure is measured with AFM, using a method similar to that in Shi et al. (21). From the AFM images, we measured the end-to-end distances of spectrins in the cytoskeleton network (Fig. 2 *b* and Fig. S3). The result shows an overall increase of the end-to-end distances after chloroquine treatment. The typical AFM images are shown in Fig. 2, *c* and *d*. The larger dark spots in Fig. 2 *d* indicate larger holes in the cytoskeletal network, consistent with our measurement of the end-to-end distances of spectrins.

Numerical calculation

For a general probability density function $\mathcal{P}(k)$, Eq. 5 can be solved numerically. Here we consider the variation of the lengths of spectrins in the network, as well as the probability of missing spectrins between nodes. Because the effective spring constant of the spectrin depends on the end-to-end distance, the length distribution introduced by Eq. 2 induces the probability distribution of elastic constants for spectrins. Combined with the probability of missing a spectrin connection ($1-p$), the probability density function of the spring constants in the cytoskeletal network can be written as

$$\mathcal{P}(k) = p^* \widetilde{\mathcal{P}}(z)\frac{dz}{dk} + (1-p)\delta(k), \quad (6)$$

where $\widetilde{\mathcal{P}}(z)$ is the distribution of the end-to-end distance z and normalized for $0 < z < L$, i.e., $\int_0^L \widetilde{\mathcal{P}}(z)dz = 1$, and $\delta(k)$ is the Dirac Delta function. In the first term on the right-hand side, $\widetilde{\mathcal{P}}(z)(dz/dk)$ gives the distribution of the spring constant k. Using the probability density function (Eq. 6), the EMT equation (Eq. 5) is rewritten as

$$\int \frac{\widetilde{\mathcal{P}}(z)}{1-\alpha(1-k(z)/k_m)}dz = \left(1-\frac{1-p}{1-\alpha}\right)\Big/ p. \quad (7)$$

As discussed earlier, the value of α depends on the geometry of, and the prestresses in, the network. Here we take the value $\alpha = 2/3$ for a stress-free triangular network (29) and solve k_m numerically. Tang and Thorpe (31) shows the relation between α and prestrain in the network. We found that changing the value of α (from 1/3 to 2/3) changes the value of k_m but does not change the qualitative dependence of k_m on p, z_0, and σ as shown in Fig. 3. Once we obtain the effective spring constant k_m for the equivalent regular network, the in-plane shear modulus μ, to the lowest order, is linearly proportional to k_m. Hence, to study how μ depends on the disorders, it is equivalent to find out the dependence of k_m on the connection formation probability p, the average end-to-end distance z_0, and the variance σ^2 of z.

Our numerical results are summarized in Fig. 3. With a fixed value of $p = 0.8$ (Fig. 3 *a*), the effective spring constant k_m increases with σ for relatively small values of z_0, but decreases with σ for relatively large values of z_0 ($z_0 \gtrsim 100$ nm). On the other hand, k_m always increases with increasing z_0 given the value of σ. This supports the prediction that the experimentally observed cell stiffening is related to the observed lengthening of spectrins in the cytoskeleton network. With fixed value of $\sigma = 30$ nm (Fig. 3 *b*), as one may expect, k_m increases with increasing z_0 given the value of p, and also increases with increasing p given the value of z_0. With a fixed value of $z_0 = 100$ nm (Fig. 3 *c*), k_m increases with increasing p given the value of σ. But similar to what is shown in Fig. 3 *a*, k_m increases with increasing σ for relatively high values of p ($p \gtrsim 0.86$) while it decreases with increasing σ for relatively low values of p. Therefore, our numerical results suggest that, given the value of p (e.g., Fig. 3 *a*) for a relatively strong network (large values of k_m), increasing the variance σ^2 of z tends to weaken the network, while for a relatively weak network (small value of k_m), increasing the variance σ^2 tends to stiffen the network. However, given a relatively medium value of z_0 (e.g., $z_0 = 100$ nm in Fig. 3 *c*), increasing σ stiffens a relatively strong network, but weakens a relatively weak network. This nontrivial dependence of k_m on σ may be utilized in cellular functions or material designs.

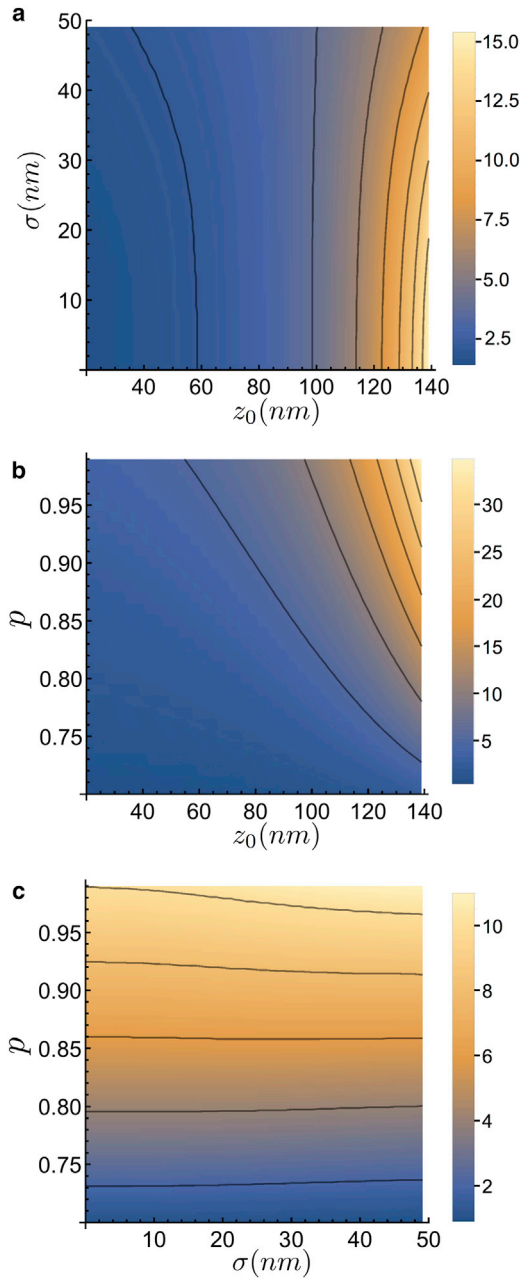

FIGURE 3 Numerical results for the effective spring constant k_m. (*a*) The dependence of k_m on z_0 and σ (Eq. 2) with the probability for one spectrin edge to present $p = 0.8$ fixed. (*b*) The dependence of k_m on z_0 and p with $\sigma = 30$ nm fixed. (*c*) The dependence of k_m on σ and p with $z_0 = 100$ nm fixed. (*Color bars*) Value of k_m in the unit of μN/m. The units match the units used in relevant experiments. To see this figure in color, go online.

Analytical solutions

Here we adopt analytical solutions from previous studies (e.g., Feng et al. (29) and Mao et al. (36)) but replace the harmonic springs with WLCs. To make the model traceable, we only consider the deviation from the regular triangular network caused by missing spectrin connections and neglect the length heterogeneity. Aiming at the dependence of shear modulus on the average spectrin length, here we will establish a correlation between the experimentally observed spectrin lengthening and cell-stiffening phenomena. In this case, the distribution function takes the following form (29,34):

$$\mathcal{P}(k') = p\delta(k' - k(z)) + (1-p)\delta(k').$$

Different from purely linear springs, stretching spectrins not only introduces internal prestresses to the network, but also increases the effective spring constants $k(z)$ of individual spectrins. If we use the average extension $\langle z \rangle$ to replace the inhomogeneous end-to-end distance z, Eq. 5 can be solved exactly (29). Again, the length-dependent spring constant only sets up the initial value of $k(z)$. After that, we treat all the spectrins as Hookean springs and k as independent of z, and only consider the linear response of the network for small perturbations. With this consideration, Eq. 5 is solved to give us

$$k_m = k(z)\frac{p-p_c}{1-p_c} = \frac{1}{\beta l_p L}\left(1+\frac{1}{2}\left(1-\frac{z}{L}\right)^{-3}\right)\frac{p-p_c}{1-p_c}. \quad (8)$$

Here we consider p as a constant independent of initial stresses. The case of a stress-dependent p will be discussed in the next section. Thus, we map the disordered network to a regular triangular network consisting of springs with a single spring constant k_m. It is clear that, in our model, cell stiffening comes directly from the nonlinearity of the WLC model, as shown by the z-dependent term on the right-hand side of Eq. 8. The macroscopic in-plane shear modulus μ of the 2D network is linearly proportional to the effective spring constant, i.e., $\mu \propto k_m$.

On the other hand, it is known that prestresses can stiffen the network (e.g., Tang and Thorpe (31), Boal et al. (33), and Sheinman et al. (34)), a similar effect to that discussed in Numerical Calculation, above. The prestress is relevant to various cell physiological processes, e.g., adhesively tensed membranes of spread cells (40), the expression and export of transmembrane proteins onto the iRBC membrane that bind to spectrins, the formation of knobs at dispersed sites on the RBC membrane that can link to near-by spectrins, the expansion of the cell's volume due to the invaded and multiplying malarial parasites, and so on. In our model, without knowing more details about the intracellular processes involved, we use a single-stress-dependent prefactor $a(P)$ to account for the influence of the prestresses on the elastic properties of the cytoskeletal network. With that in mind, the shear modulus of the 2D network is given by

$$\mu = a(P)k_m = \frac{a(P)}{\beta l_p L}\left(1+\frac{1}{2}\left(1-\frac{z}{L}\right)^{-3}\right)\frac{p-p_c}{1-p_c}, \quad (9)$$

where P is the prestress in the network, defined to be negative for networks under tension.

Fig. 4 *a* shows our analytical results for different values of p_c. We focus on the dependence of the shear modulus μ on the average end-to-end distance z_0 and we use $p = 0.55$, which is approximated from our AFM measurements. Qualitatively, it is clear that the shear modulus of the network increases with increasing average end-to-end length z_0 of the spectrins in the network. By adjusting the value of p_c and $a(P)$, our results agree well with experiments (*red dots* with error bars in Fig. 4 *a*). The comparison with experiments is elaborated below.

Comparison with experiments

Equation 9 is used to compare with experiments. By using the micropipette aspiration technique, we found that the malaria iRBCs become stiffer after chloroquine treatment (Fig. 2 *a*). In the meantime, through AFM measurements, we found that the average end-to-end distance of spectrins in the cytoskeleton increases after the drug treatment (Fig. 2 *b*). This coincidence is also noticed in iRBCs at different stages of malaria infection (17-21). In our experiments, both the shear modulus μ and the spectrin lengths were measured (Fig. 4 *a*), and the data showed a positive correlation between these two quantities. In addition, the average connectivity is also obtained, which is ~3.3 across several samples. So we use this number to determine the value of $p \approx 3.3/6 = 0.55$ in our model. For other parameters, we use $L = 200$ nm, $T = 300$ K, and $l_p = 10$ nm, which agree with the values reported in the experiments or in the literature (41-43). The values a and p_c are used as fitting parameters. Using the values $a = 15$ and $p_c = 0.45$, our results (Eq. 9) agree well with the experimental observations (Fig. 4 *a* and the *inset*). For the black curve in the inset of Fig. 4, the mean values of the lengths of spectrins at different times are used in Eq. 9 to obtain the respective values of μ. Due to the relatively large error bars in the experiments, the values of a and p_c can vary in a certain range. Better estimations of the parameter values are worthy of further investigations and more precise experimental measurements in our future work. However, the agreement supports the prediction that the shear modulus of the network is largely affected by the average length of edges (e.g., spectrins) in the cytoskeletal network.

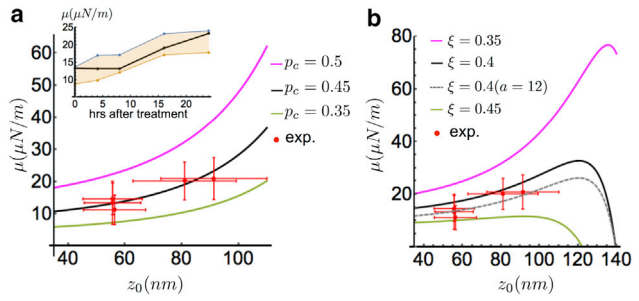

FIGURE 4 Analytical results and comparison with experiments. (*a*) Dependence of the shear modulus μ on the average end-to-end distance z_0. (*Red dots* with *error bars*) Experimental data. Different curves correspond to different values of p_c. (*Inset*) Comparison between the analytical result and the experiments. (*Black curve*) Analytical result, taking the same parameters as the black curve in (*a*) ($p_c = 0.45$). (*Shaded area*) 90% pointwise confidence band for the experimentally obtained mean values of the shear modulus. (*b*) Nonmonotonic dependence of μ on z_0 for different values of ξ (Eq. 10), when the unbinding kinetics is taken into account. To see this figure in color, go online.

DISCUSSION

Several questions deserve further discussions here. Firstly, the binding/unbinding kinetics between spectrins and the nodes (protein complexes) can be force-dependent. Here we simply assume an exponential dependence of the edge-missing probability on the force, i.e., $(1-p) \sim (\beta x^{\#} f)$, where $f = f(z)$ depends on the end-to-end distances of the spectrins as in Eq. 3. By plugging in $p = 1 - \xi\exp(\beta x^{\#} f(z))$ in Eq. 9, we obtain

$$\mu = \frac{a(P)}{\beta l_p L}\left(1 + \frac{1}{2}\left(1 - \frac{z}{L}\right)^{-3}\right)\frac{(1 - \xi\exp(\beta x^{\#} f(z))) - p_c}{1 - p_c}, \tag{10}$$

where $x^{\#}$ is a parameter describing the length scale between the binding potential minimum and maximum. In Eq. 10, z is approximated as the average end-to-end distance $\langle z \rangle$. Two competing effects are immediately noticed from Eq. 10. The $(1 + (1/2)(1 - (z/L))^{-3})$ term coming from the WLC model predicts cell stiffening due to lengthening of spectrins, while the other term $1 - \xi\exp(\beta x^{\#} f(z))$ weakens the network. For relatively short spectrin lengths, the cell stiffens due to the stiffening of spectrins as their lengths are increased. However, at large spectrin lengths that may be beyond the measurements of current experiments, the weakening term dictates the elastic properties of the network and the bond-forming probability p may even drop below the rigidity percolation threshold p_c. Thus a turning point should be observed if the length of the spectrins keep increasing, dividing the two different dependences of shear modulus on z. Fig. 4 *b* confirms this prediction, and shows the dependence of the shear modulus μ on the average end-to-end distance z_0 of the spectrins for different values of ξ. In Fig. 4 *b*, we use $x^{\#} = 1$ nm that is in the range of values for similar problems (15) and $p_c = 0.45$. Other parameters take the same values as those for Fig. 4 *a*. The curves in Fig. 4 *b* are slightly shifted from those in Fig. 4 *a* due to the differences between Eqs. 9 and 10. The agreement with experiments (*red dots* with *error bars*) can be retained by only slightly changing the value of a ($a = 12$ for the *gray dashed curve* in Fig. 4 *b*) with other parameters staying the same. Having that said, here we are more interested in the qualitative nonmonotonic dependence of μ on z_0, while the exact shape of the curve needs to be further determined by parameters from future experimental

investigations. In addition, more quantitative experimental studies on the relation between the cytoskeleton structure and the shear modulus should include measurements of the two quantities under the same conditions, for example, both in liquid (with liquid mode AFM (44)) or for live cells.

Secondly, it is noted that prestress can significantly alter the geometry or topology of the network through stretching of spectrins. Membrane tension is relevant to various cell physiological processes. For example, in iRBCs, after the malaria infection, knobs are expressed across the membrane, which are complexes of malarial-parasite-exported proteins. These knobs are found capable of binding to spectrins and can possibly introduce stresses in the cytoskeletal network (21) by stretching spectrins. In our study of chloroquine-treated iRBCs, the increased prestress in the cytoskeleton is inferred from the increased length of the spectrins. Such a correlation is also observed in the study of adhesively tensed membranes of spread cells (40). As shown in previous studies, in iRBCs with chloroquine treatment, the oxidative stress that resulted from the drug treatment can be responsible for the change of mechanical properties of the cytoskeleton (6,8). We suspect that this oxidative stress may be related to the formation of new protein complexes that bind to spectrins, and subsequently generate stresses in the network. In this case, the effect of chloroquine treatment is partially impaired by the continuous stiffening of the cells, because stiffer cells are sometimes easier to block the blood circulation. Further experimental investigations of the origin of the stresses and their effects will improve our understanding of the mechanism of fatal diseases and drug treatments.

From a broader perspective, although here we looked at the 2D network, especially the RBC cytoskeleton as an example, our model in general bridges the properties of biopolymers at the molecular level and the elastic properties at the cellular level. Similar models may be extended to other dimensions and shapes. Our results also show a possible mechanism for cells to adjust their stiffness from the molecular level and may stimulate new ideas in material designs.

CONCLUSIONS

To conclude, we investigated the relationship between the network structure and its stiffness. We focused on how the disorders introduced to a regular 2D triangular network affected its macroscopic in-plane shear modulus. By applying the WLC model to single spectrins that form the edges of the network, we found that the shear modulus of the network increased with the average length of the spectrins. Our result agrees with previous studies in that removing some edges with probability $1-p$ weakens the network, which shows a competing effect with the stiffening caused by lengthening of spectrins (WLCs). On the other hand, as discussed in the Results, depending on the values of the average length z_0 or p, the shear modulus may increase or decrease with increasing variance (σ^2) of the length distribution (Fig. 3, *a–c*). Furthermore, if the stress-dependent binding/unbinding kinetics is taken into account, the shear modulus has a first-increase-then-decrease behavior as the average length of the spectrins increases. More importantly, our results agree well with recent experimental observations for malaria-iRBCs, which shows a correlation between the lengthening of spectrins (edges of the cytoskeleton network) and stiffening of the cells (increase of shear modulus). Further investigations of what causes the lengthening of spectrins or the internal stresses in the cytoskeleton will be valuable in identifying new treatment methods or targeted therapy for RBC-related diseases, such as malaria infection.

SUPPORTING MATERIAL

Four figures are available at http://www.biophysj.org/biophysj/supplemental/S0006-3495(15)01112-1.

AUTHOR CONTRIBUTIONS

L.L, X.X., C.T.L., and J.C. designed the research; L.L. and X.X. performed the research; and L.L., C.T.L., and J.C. wrote the article.

ACKNOWLEDGMENTS

We acknowledge the financial assistance of the Singapore-Massachusetts Institute of Technology Alliance for Research and Technology, and the National Science Foundation (under grant No. CHE-1112825).

REFERENCES

1. Discher, D. E., N. Mohandas, and E. A. Evans. 1994. Molecular maps of red cell deformation: hidden elasticity and in situ connectivity. *Science.* 266:1032–1035.
2. Suresh, S. 2006. Mechanical response of human red blood cells in health and disease: some structure-property-function relationships. *J. Mater. Res.* 21:1871–1877.
3. Broedersz, C. P., and F. C. MacKintosh. 2014. Modeling semiflexible polymer networks. *Rev. Mod. Phys.* 86:995–1036.
4. Xu, K., G. Zhong, and X. Zhuang. 2013. Actin, spectrin, and associated proteins form a periodic cytoskeletal structure in axons. *Science.* 339:452–456.
5. Lai, L., and J. Cao. 2014. Spectrins in axonal cytoskeletons: dynamics revealed by extensions and fluctuations. *J. Chem. Phys.* 141:015101.
6. Huang, S., A. Amaladoss, …, J. Han. 2014. In vivo splenic clearance correlates with in vitro deformability of red blood cells from *Plasmodium yoelii*-infected mice. *Infect. Immun.* 82:2532–2541.
7. Lenormand, G., S. Hénon, …, F. Gallet. 2001. Direct measurement of the area expansion and shear moduli of the human red blood cell membrane skeleton. *Biophys. J.* 81:43–56.
8. Hale, J. P., C. P. Winlove, and P. G. Petrov. 2011. Effect of hydroperoxides on red blood cell membrane mechanical properties. *Biophys. J.* 101:1921–1929.
9. Saxton, M. J. 1990. The membrane skeleton of erythrocytes. A percolation model. *Biophys. J.* 57:1167–1177.
10. Boal, D. H. 1994. Computer simulation of a model network for the erythrocyte cytoskeleton. *Biophys. J.* 67:521–529.

11. Hansen, J. C., R. Skalak, …, A. Hoger. 1997. Influence of network topology on the elasticity of the red blood cell membrane skeleton. *Biophys. J.* 72:2369–2381.
12. Boey, S. K., D. H. Boal, and D. E. Discher. 1998. Simulations of the erythrocyte cytoskeleton at large deformation. I. Microscopic models. *Biophys. J.* 75:1573–1583.
13. Gov, N. S. 2007. Less is more: removing membrane attachments stiffens the RBC cytoskeleton. *New J. Phys.* 9:429.
14. Byers, T. J., and D. Branton. 1985. Visualization of the protein associations in the erythrocyte membrane skeleton. *Proc. Natl. Acad. Sci. USA.* 82:6153–6157.
15. Efremov, A., and J. Cao. 2011. Bistability of cell adhesion in shear flow. *Biophys. J.* 101:1032–1040.
16. Xu, X., A. K. Efremov, …, J. Cao. 2013. Probing the cytoadherence of malaria infected red blood cells under flow. *PLoS One.* 8:e64763.
17. Chien, S., K.-L. P. Sung, …, A. Tözeren. 1978. Theoretical and experimental studies on viscoelastic properties of erythrocyte membrane. *Biophys. J.* 24:463–487.
18. Nash, G. B., E. O'Brien, …, J. A. Dormandy. 1989. Abnormalities in the mechanical properties of red blood cells caused by *Plasmodium falciparum*. *Blood.* 74:855–861.
19. Paulitschke, M., and G. B. Nash. 1993. Membrane rigidity of red blood cells parasitized by different strains of *Plasmodium falciparum*. *J. Lab. Clin. Med.* 122:581–589.
20. Glenister, F. K., R. L. Coppel, …, B. M. Cooke. 2002. Contribution of parasite proteins to altered mechanical properties of malaria-infected red blood cells. *Blood.* 99:1060–1063.
21. Shi, H., Z. Liu, …, C. T. Lim. 2013. Life cycle-dependent cytoskeletal modifications in *Plasmodium falciparum* infected erythrocytes. *PLoS One.* 8:e61170.
22. Hughes, K. R., G. A. Biagini, and A. G. Craig. 2010. Continued cytoadherence of *Plasmodium falciparum* infected red blood cells after antimalarial treatment. *Mol. Biochem. Parasitol.* 169:71–78.
23. Trager, W., and J. B. Jensen. 1976. Human malaria parasites in continuous culture. *Science.* 193:673–675.
24. Ribaut, C., A. Berry, …, A. Valentin. 2008. Concentration and purification by magnetic separation of the erythrocytic stages of all human *Plasmodium* species. *Malar. J.* 7:45.
25. Bell, G. I. 1978. Models for the specific adhesion of cells to cells. *Science.* 200:618–627.
26. Marko, J. F., and E. D. Siggia. 1995. Stretching DNA. *Macromolecules.* 28:8759–8770.
27. Yang, S., J. B. Witkoskie, and J. Cao. 2003. First-principle path integral study of DNA under hydrodynamic flows. *Chem. Phys. Lett.* 377: 399–405.
28. Xu, X., B. J. R. Thio, and J. Cao. 2014. Correlated local bending of a DNA double helix and its effect on DNA flexibility in the sub-persistence-length regime. *J. Phys. Chem. Lett.* 5:2868–2873.
29. Feng, S., M. F. Thorpe, and E. Garboczi. 1985. Effective-medium theory of percolation on central-force elastic networks. *Phys. Rev. B Condens. Matter.* 31:276–280.
30. Thorpe, M. F., and E. J. Garboczi. 1990. Elastic properties of central-force networks with bond-length mismatch. *Phys. Rev. B Condens. Matter.* 42:8405–8417.
31. Tang, W., and M. F. Thorpe. 1988. Percolation of elastic networks under tension. *Phys. Rev. B Condens. Matter.* 37:5539–5551.
32. Boal, D. H., U. Seifert, and J. C. Shillcock. 1993. Negative Poisson ratio in two-dimensional networks under tension. *Phys. Rev. E Stat. Phys. Plasmas Fluids Relat. Interdiscip. Topics.* 48:4274–4283.
33. Boal, D. H. 1998. Two-dimensional cytoskeletons under stress. *Biol. Bull.* 194:331–333.
34. Sheinman, M., C. P. Broedersz, and F. C. MacKintosh. 2012. Nonlinear effective-medium theory of disordered spring networks. *Phys. Rev. E Stat. Nonlin. Soft Matter Phys.* 85:021801.
35. Das, M., F. C. MacKintosh, and A. J. Levine. 2007. Effective medium theory of semiflexible filamentous networks. *Phys. Rev. Lett.* 99:038101.
36. Mao, X., O. Stenull, and T. C. Lubensky. 2013. Effective-medium theory of a filamentous triangular lattice. *Phys. Rev. E Stat. Nonlin. Soft Matter Phys.* 87:042601.
37. Broedersz, C. P., C. Storm, and F. C. MacKintosh. 2009. Effective-medium approach for stiff polymer networks with flexible cross-links. *Phys. Rev. E Stat. Nonlin. Soft Matter Phys.* 79:061914.
38. Evans, E. A. 1973. New membrane concept applied to the analysis of fluid shear- and micropipette-deformed red blood cells. *Biophys. J.* 13:941–954.
39. Hochmuth, R. M. 2000. Micropipette aspiration of living cells. *J. Biomech.* 33:15–22.
40. Hategan, A., R. Law, …, D. E. Discher. 2003. Adhesively-tensed cell membranes: lysis kinetics and atomic force microscopy probing. *Biophys. J.* 85:2746–2759.
41. Stokke, B. T., A. Mikkelsen, and A. Elgsaeter. 1985. Human erythrocyte spectrin dimer intrinsic viscosity: temperature dependence and implications for the molecular basis of the erythrocyte membrane free energy. *Biochim. Biophys. Acta.* 816:102–110.
42. Svoboda, K., C. F. Schmidt, …, S. M. Block. 1992. Conformation and elasticity of the isolated red blood cell membrane skeleton. *Biophys. J.* 63:784–793.
43. Li, J., M. Dao, …, S. Suresh. 2005. Spectrin-level modeling of the cytoskeleton and optical tweezers stretching of the erythrocyte. *Biophys. J.* 88:3707–3719.
44. Liu, F., J. Burgess, …, A. Ostafin. 2003. Sample preparation and imaging of erythrocyte cytoskeleton with the atomic force microscopy. *Cell Biochem. Biophys.* 38:251–270.